

# Magnetohydrodynamics equilibria with toroidal and poloidal flow<sup>a)</sup>

L. Guazzotto<sup>b)</sup> and R. Betti

*University of Rochester and Laboratory for Laser Energetics, Rochester, New York 14623*

(Received 19 November 2004; accepted 20 December 2004; published online 7 April 2005)

In the present work, the effects of flow on tokamak equilibria are investigated, focusing in particular on the effects of poloidal flows. It is shown that discontinuous transonic equilibria with a pedestal structure can be obtained for relatively low values of the poloidal velocity. Equilibria with poloidal flow of the order of the poloidal Alfvén speed are shown to develop inverted Shafranov shift. Since the rotation is damped by the neoclassical poloidal viscosity, a quasi-omnigenous solution for equilibria with large rotation is also derived in order to minimize the flow damping. In this solution, the magnetic field is construed to be a function of the poloidal magnetic flux  $\Psi$  up to a small correction by an appropriate choice of the flow profiles. All numerical results are obtained with the code FLOW [L. Guazzotto, R. Betti, J. Manickam, and S. Kaye, *Phys. Plasmas* **11**, 604 (2004)].

© 2005 American Institute of Physics. [DOI: 10.1063/1.1869502]

## I. INTRODUCTION

In recent years, much effort has been devoted to investigate the properties of tokamak plasmas in the presence of macroscopic flow. The increasing focus of both theoretical and experimental research on this topic has been mostly driven by the experimental observations of the last generation of tokamaks, indicating that poloidal and toroidal plasma rotation can be routinely obtained in experiments, such as the Electric Tokamak (ET),<sup>1</sup> the Joint European Torus,<sup>2</sup> DIII-D<sup>3</sup>, and the National Spherical Tokamak Experiment.<sup>4</sup> The presence of macroscopic flow significantly alters both equilibrium and stability properties of tokamak plasma. However, little effort has been devoted to the development of equilibrium codes including plasma flow. To the authors' knowledge, only three codes include poloidal flow in the equilibrium calculations, CLIO,<sup>5</sup> FINESSE,<sup>6</sup> and FLOW.<sup>7</sup> No code has however been used to investigate the dramatic qualitative changes in the equilibrium properties of tokamaks caused by poloidal flow, except for the code FLOW.<sup>7</sup>

In the present work, we will focus on the study of the changes in equilibrium properties caused by the presence of flow. If the poloidal flow is in the range of the poloidal sound speed  $C_{s\theta} \equiv C_s B_\theta / B$ , a dramatic change in the equilibrium occurs, as the poloidal flow jumps from subsonic to supersonic at the transonic surface, and density and pressure profiles develop a sharp discontinuity leading to a pedestal structure. Discontinuous equilibria are the only solution to the Grad–Shafranov–Bernoulli system in the presence of transonic poloidal flows, which can occur near the plasma edge, where  $C_{s\theta}$  is small and even a relatively slow flow can become transonic. Another dramatic change in the equilibrium properties occurs when the poloidal velocity is of the order of the poloidal Alfvén speed. In that case, the equilibrium profiles will again be continuous, but the Shafranov

shift of the magnetic surfaces will be directed inward. This inward shift causes an enhancement of the dynamic forces that counterbalance the outward-pointing pressure forces. As these equilibria require a large poloidal flow, it is also appropriate to address the issue of poloidal viscosity. As the poloidal viscosity in tokamaks is due to the effect of magnetic pumping, it depends on the magnetic field strength variations along a magnetic surface. For this reason, a new class of quasi-omnigenous equilibria, for which  $|B| \approx |B|(\Psi) + O(\epsilon^2)$ , is described.

The present work is organized as follows. In Sec. II a brief review of the theory of equilibria with flow, and of the numerical solution with the code FLOW, is given. In Sec. III, transonic equilibria with poloidal flow of the order of the poloidal sound speed are presented. In Sec. IV, the general theory of equilibria with poloidal velocity exceeding the poloidal Alfvén speed is discussed in detail. In Sec. V, a new class of quasi-omnigenous equilibria with fast poloidal flow is described.

## II. THE EQUILIBRIUM PROBLEM

The derivation of the equilibrium equations for flowing magnetohydrodynamics (MHD) plasmas has been extensively discussed in the literature (see, e.g., Refs. 8,9), and the details of the numerical solution with the code FLOW have been described in Ref. 7. Both issues are therefore only very briefly summarized here.

The equilibrium equations are derived starting from the usual fluid MHD equations, namely, mass and momentum conservation, and the equilibrium Maxwell equations, with the addition of Ohm's law. The crucial assumptions include axisymmetry, negligible plasma resistivity and viscosity, and a closure equation for the plasma pressure. By using the usual set of cylindrical coordinates  $(R, \varphi, Z)$  and decomposing the magnetic field in a toroidal (aligned with  $\varphi$ ) and a divergence-free poloidal component expressed as  $\underline{B}_\theta = (\nabla\Psi \times \hat{e}_\varphi)/R$ , the closure equation can be expressed as

<sup>a)</sup>Paper E11 5, *Bull. Am. Phys. Soc.* **49**, 99 (2004).

<sup>b)</sup>Invited speaker.

TABLE I. Physical meaning of the “intuitive” free functions.

Function	Physical meaning
$D(\Psi)$	Quasi-density
$P(\Psi)$	Quasi-isotropic pressure
$B_0(\Psi)$	Quasi-toroidal component of the magnetic field
$M_\varphi(\Psi)$	Quasi-toroidal sonic Mach number
$M_\theta(\Psi)$	Quasi-poloidal sonic Mach number

$$p = S(\Psi)\rho^\gamma, \quad (1)$$

where  $S(\Psi)$  is a free function of  $\Psi$ , representing either the plasma entropy, if  $\gamma=5/3$ , or the plasma temperature, if  $\gamma=1$ . The flow is expressed by the general equations:

$$v_\theta = \frac{\Phi(\Psi)}{\sqrt{\mu_0\rho}} B_\theta, \quad v_\varphi = \frac{\Phi(\Psi)}{\sqrt{\mu_0\rho}} B_\varphi + R\Omega(\Psi) \quad (2)$$

while the toroidal component of the magnetic field is written as

$$B_\varphi R = \frac{F(\Psi) + \sqrt{\mu_0} R^2 \Phi(\Psi) \Omega(\Psi)}{1 - \Phi^2(\Psi)/\rho}. \quad (3)$$

By the use of the previous equations, the equilibrium problem can be written as a system of two coupled equations:

$$\frac{1}{2\mu_0} \left[ \frac{\Phi(\Psi)B}{\rho} \right]^2 - \frac{1}{2} [R\Omega(\Psi)]^2 + W = H(\Psi), \quad (4)$$

$$\begin{aligned} \nabla \cdot \left[ (1 - M_{A\theta}^2) \left( \frac{\nabla \Psi}{R^2} \right) \right] = & - \frac{B_\varphi}{R} \frac{dF(\Psi)}{d\Psi} - \frac{\vec{v} \cdot \vec{B}}{\sqrt{\mu_0}} \frac{d\Phi(\Psi)}{d\Psi} \\ & - R\rho v_\varphi \frac{d\Omega(\Psi)}{d\Psi} - \rho \frac{dH(\Psi)}{d\Psi} \\ & + \frac{\rho^\gamma}{\gamma-1} \frac{dS(\Psi)}{d\Psi}, \end{aligned} \quad (5)$$

i.e., the (algebraic) Bernoulli and the (PDE) Grad–Shafranov (GS) equation, where  $M_{A\theta} = \Phi(\Psi)/\sqrt{\rho}$  is the poloidal Alfvénic Mach number and  $W = [\gamma/(\gamma-1)]S(\Psi)\rho^{\gamma-1}$  is the plasma enthalpy. Before the equilibrium problem can be solved, it is necessary to assign the free functions:

$$F(\Psi), H(\Psi), S(\Psi), \Omega(\Psi), \Phi(\Psi). \quad (6)$$

That is done in a way described in detail in Ref. 7. Just for convenience, the tables describing the physical meaning of the “input” free functions and the relations between the two sets of free functions are reproduced here in Tables I and II from Ref. 7, limited to the ones relevant to the MHD closure. All the quasifunctions in Table I approach the corresponding physical variables in the infinite aspect ratio limit.

As for the numerical solution of the equilibrium problem, that is also detailed in Ref. 7. Let us just remind the reader that FLOW uses a multigrid solver, which iteratively solves Eqs. (4) and (5).

TABLE II. Relation between the two sets of free functions.  $R_0$  is the position of the geometric axis of the plasma.

Function	Definition
$F(\Psi)$	$R_0 B_0(\Psi)$
$\Phi(\Psi)$	$\sqrt{\gamma P(\Psi) D(\Psi)} \frac{M_\theta(\Psi)}{B_0(\Psi)}$
$\Omega(\Psi)$	$\sqrt{\gamma \frac{P(\Psi)}{D(\Psi)} \frac{M_\varphi(\Psi) - M_\theta(\Psi)}{R_0}}$
$H(\Psi)$	$\frac{P(\Psi)}{D(\Psi)} \left[ \frac{1}{\gamma-1} + M_\theta(\Psi) M_\varphi(\Psi) - \frac{1}{2} M_\varphi^2(\Psi) \right]$
$S(\Psi)$	$\frac{P(\Psi)}{[D(\Psi)]^\gamma}$

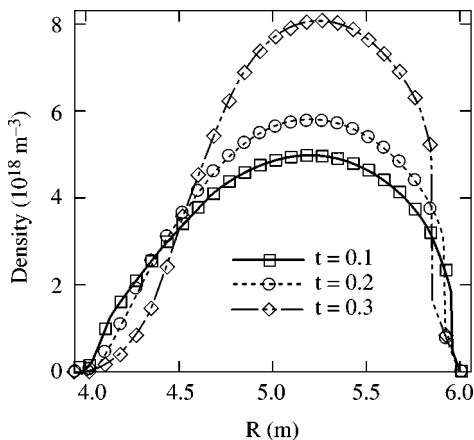
### III. EQUILIBRIA WITH TRANSONIC POLOIDAL FLOW

The problem of the numerical solution of equilibria with transonic poloidal flow has been described in Ref. 7, where it has been shown that, as predicted by Ref. 10, those equilibria exhibit discontinuous profiles for all plasma properties. The reason of this unusual behavior is in the bifurcation occurring in the solution of the Bernoulli equation between a subsonic and a supersonic root as the distance between any two magnetic surfaces varies along the poloidal angle.

In addition to the discussion of Ref. 7 for this class of equilibria, we intend to emphasize the fact that transonic equilibria do not require large poloidal velocities in order to exist. As the poloidal sound speed vanishes at the plasma edge, a relatively small velocity can be sufficient to originate transonic equilibria. Moreover, the required velocity will depend on the position of the transonic surface, becoming smaller as the transonic surface gets closer to the plasma edge. In order to show this, a parameter is introduced in the free function assigning the poloidal flow  $M_\theta(\Psi)$ , which is defined as follows:

$$\begin{aligned} M_\theta(\Psi) = & M_\theta^{\max} \left[ \frac{2}{t} \left( \frac{\Psi}{\Psi_c} \right) - \frac{1}{t^2} \left( \frac{\Psi}{\Psi_c} \right)^2 \right] \quad \text{if } \Psi \leq \Psi_t \\ & M_\theta^{\max} \left[ \frac{1}{(t-1)^2} \left( 1 - \frac{\Psi}{\Psi_c} \right) \left( \frac{\Psi}{\Psi_c} + 1 - 2t \right) \right] \quad \text{if } \Psi \geq \Psi_t. \end{aligned} \quad (7)$$

Here,  $t \equiv \Psi_t/\Psi_c$  is a free parameter used to control the position of the transonic surface, with  $\Psi_t$  corresponding to the value of the poloidal magnetic flux  $\Psi$  where the transonic surface is positioned, while  $\Psi_c$  is the magnetic flux at the magnetic axis and  $\Psi=0$  corresponds to the plasma edge. A small  $t$  will therefore force the transonic surface to be close to the edge, while the opposite will be true for a large  $t$ . Equation (7) assures that  $M_\theta(\Psi)$ , as well as its first deriva-

FIG. 1. Density profile in ET-like transonic equilibria for varying  $t$ .

tive, will be continuous for  $0 < \Psi < \Psi_c$ . The definition of  $t$  obviously requires  $0 < t < 1$ .

Quasidensity  $D(\Psi)$  and quasipressure  $P(\Psi)$  are assigned as power laws, while the quasitoroidal magnetic field  $B_0(\Psi)$  is defined in terms of  $P(\Psi)$ , as indicated below, and finally the quasitoroidal sonic Mach number  $M_\varphi$  is set equal to 0:

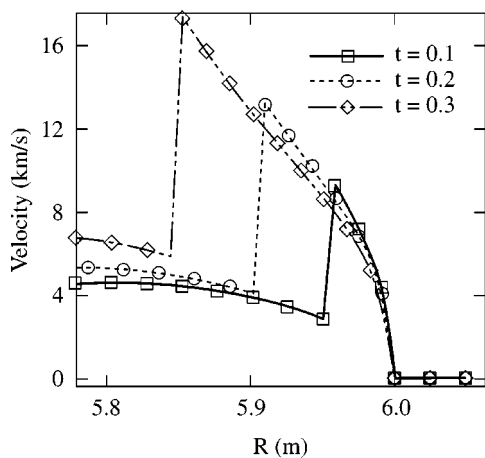
$$D(\Psi) \equiv D^E + (D^C - D^E) \left( \frac{\Psi}{\Psi_c} \right)^{\alpha_p}, \quad (8)$$

$$P(\Psi) \equiv P^E + (P^C - P^E) \left( \frac{\Psi}{\Psi_c} \right)^{\alpha_p}, \quad (9)$$

$$R_0 B_0(\Psi) = \sqrt{F_V^2 - \mu_0 P(\Psi) R_0^2}, \quad (10)$$

where  $\alpha_p = 0.5$  and  $\alpha_p = 1.5$  have been chosen in order to obtain a fairly flat density profile and a fairly peaked pressure profile.  $D^C$  and  $P^C$  obviously correspond to the values of the free functions at the magnetic axis, while  $D^E \ll D^C$  and  $P^E \ll P^C$  correspond to the edge values of the free functions.

Numerical results relative to transonic equilibria obtained with the code FLOW for three different values of  $t$  ( $t=0.1$ ,  $t=0.2$ , and  $t=0.3$ ) are presented in Figs. 1 and 2. The plasma geometry has been defined to reproduce data

FIG. 2. Poloidal velocity profile in ET-like transonic equilibria for varying  $t$ , transonic surface zoom.

relevant to the ET,<sup>1</sup> with  $R_0=5$ ,  $a=1$ , and  $\kappa=2$ . The chosen input free functions correspond to a low  $\beta$  equilibrium, with toroidal  $\beta$  ( $\beta_t \equiv 2\langle p \rangle / B_V^2$ )  $\sim 1\%$ . These equilibria have been obtained by assigning all input free functions, and then adjusting the pressure peak  $P^C$  in Eq. (9) in order to keep constant the total plasma thermal energy  $(3/2) \int p dV$ , and adjusting  $D^C$  in order to keep constant the total plasma mass. The spatial resolution used to obtain this set of equilibria is  $256 \times 256$  points. Figure 1 contains line cuts of density profiles for the three equilibria. Each profile presents a radial discontinuity in the outboard side of the plasma region, the size and location of which depend on the value of  $t$ . More precisely, the discontinuity is closer to the edge for smaller  $t$ , as expected. It can also be noted that the height of the jump is smaller when the discontinuity is closer to the edge, larger when it is farther from the edge. This is naturally due to the fact that the free function  $D(\Psi)$  is smaller near the edge, because the transonic jump actually determines a discontinuity in  $\rho/D$ , as explained in detail in Ref. 10.

It seems worthwhile to examine in some detail the poloidal velocity profiles corresponding to the equilibria under discussion. In particular, since the velocities will be largest on the outboard side of the plasma, we will only look at a closeup of the velocity profiles next to the transonic surface in that region. This is presented in Fig. 2. It is immediately apparent that poloidal velocities become larger if  $t$  is increased with all other relevant conditions kept unchanged. It is also easy to recognize the “jumps” in the poloidal velocity occurring at the same radial locations as the discontinuities in the density profiles shown in Fig. 1, i.e., again at the transonic surface. In the figure, it is easy to recognize the maximum value of the poloidal velocity in each one of the three equilibria presented in this section. In particular, the equilibrium corresponding to  $t=0.1$  (i.e., the equilibrium with the transonic surface closest to the edge) shows a maximum poloidal velocity of  $\sim 9$  km/s, the one corresponding to  $t=0.3$  (i.e., the one with the transonic surface farthest from the edge among the three considered) shows a maximum poloidal velocity of  $\sim 17$  km/s, and the equilibrium with  $t=0.2$  shows an intermediate maximum velocity of  $\sim 14$  km/s. Another interesting point that can be recognized from Fig. 2 is that the poloidal velocity in equilibria with the transonic surface closer to the edge not only has a lower maximum but it also appears to be smaller in the central portion of the plasma (this is confirmed by a full plot of the velocities). Indeed, it is easy to verify numerically that the total kinetic energy of the plasma required to create a transonic equilibrium will be smaller if the transonic surface is closer to the plasma edge.

As a conclusion to the present section, it is worth mentioning that the GS equation is hyperbolic in a very narrow range of values around  $M_{s\theta}=1$ . As discussed in Ref. 7 this does however not constitute a problem for the numerical solution of transonic equilibria, as long as the local  $\beta$  is sufficiently small.

#### IV. EQUILIBRIA WITH POLOIDAL VELOCITY EXCEEDING THE POLOIDAL ALFVÉN VELOCITY

In the present and following section, a new class of equilibria will be considered, characterized by a fast poloidal bulk rotation. More precisely, we will consider equilibria, in which the poloidal flow is super-Alfvénic with respect to the poloidal Alfvén velocity,  $V_{A\theta}^2 \equiv B_\theta^2 / \mu_0 \rho$ . The poloidal Alfvénic Mach number and the sonic poloidal Mach number are obviously related by  $M_{A\theta}^2 = M_{s\theta}^2 \beta \gamma / 2$ , where  $\beta$  is defined as  $\beta \equiv 2\mu_0 \rho / B^2$  and  $\gamma$  is the adiabatic index.

It is well known that poloidal bulk rotation is heavily damped in tokamak plasmas. It has, however, been pointed out in the literature<sup>11</sup> that the damping rate, roughly proportional to the ion-ion collision rate  $\nu_{ii}$ , is reduced for fast rotations, more precisely as the inverse square of the poloidal sonic Mach number.<sup>12</sup> Despite the reduced damping rate, sustaining fast poloidal flows will likely require a powerful source of momentum. The requirements on the momentum source are relaxed if the equilibria have an omnigenous (or quasi-omnigenous) magnetic field structure. In this section, first a simple model is considered for the fast-flowing equilibria, which is not quasi-omnigenous. The conditions for quasiomnigenity are then identified in the following section, and a new class of quasi-omnigenous equilibria is numerically computed.

##### A. The analytic model

A simple analytic model can be derived for fast-flowing plasmas, using an expansion in the inverse aspect ratio  $\epsilon$ . The main concepts of the expansion used here are contained in a model derived in Refs. 13,14, which will be modified to include the effect of poloidal flow. The basic assumptions are those of large aspect ratio ( $\epsilon \ll 1$ ), high  $\beta$  ( $\beta \sim \epsilon$ ), large poloidal flow ( $v_\varphi \ll v_\theta$ ), and constant poloidal Alfvénic Mach number, in addition to the usual assumption of axisymmetry. For convenience the plasma is also assumed to have circular cross section of minor radius  $a$ . The previous assumptions allow to write the GS equation in the following form:

$$(1 - M_{A\theta}^2) \nabla^2 \Psi_0 \simeq -R_0^2 B_0^2 \left[ \frac{B'_{\varphi 2}(\Psi_0)}{B_V} + \frac{2\mu_0 P'_1(\Psi_0)}{B_V^2} \left( \frac{r}{R_0} \right) \cos(\theta) \right], \quad (11)$$

where the prime denotes a derivation with respect to  $\Psi_0$ . Equation (11) is only valid to lowest order in  $\epsilon$ . The first two orders of the GS equation have been used to rewrite the free functions  $P(\Psi)$  and  $F(\Psi)$  (following Ref. 13) as

$$P(\Psi) = P_1(\Psi_0) \quad (12)$$

$$F(\Psi)^2 = R_0^2 B_V^2 \left[ 1 - \frac{2\mu_0 P_1(\Psi_0)}{B_V} + \frac{2B_{\varphi 2}(\Psi_0)}{B_V} \right],$$

where the subscripts indicate the ordering in  $\epsilon$ , e.g.,  $B_{\varphi 2} / B_V \sim \epsilon^2$ ,  $\Psi_0$  is the lowest order solution of the GS equation,  $R_0$  is the major radius of the plasma, and  $B_V$  is the vacuum toroidal magnetic field. In the following, it will be more convenient to assign  $B_{\varphi 2}(\Psi)$  instead of  $F(\Psi)$ . From now on, the usual set of cylindrical coordinates  $(r, \theta, z)$  will

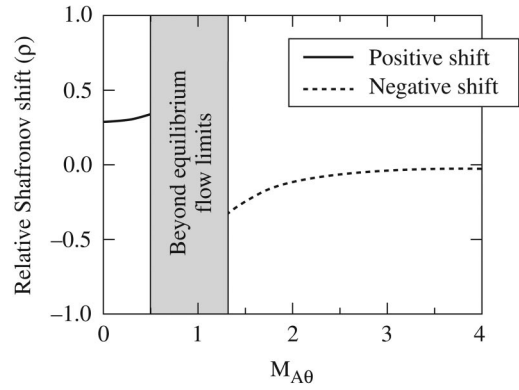


FIG. 3. Shafranov shift as a function of  $M_{A\theta}$ .

be used, with  $z$  corresponding to the toroidal (ignorable) coordinate to lowest order in  $\epsilon$ . An exact solution of Eq. (11) can be found if the free functions of  $\Psi_0$  are assigned to be linear:<sup>13</sup>

$$R_0^2 B_V B'_{\varphi 2}(\Psi_0) = -A, \quad 2\mu_0 R_0 P'_1(\Psi_0) = -C, \quad (13)$$

where  $A$  and  $C$  are so far unspecified constants. A straightforward manipulation of the GS equation yields the following form of the flux function (dropping the suffix 0 for convenience):

$$\Psi = -\frac{a^2 B_V}{q_*} \left[ (\rho^2 - 1) + \frac{\nu}{\mu} (\rho^3 - \rho) \cos(\theta) \right], \quad (14)$$

where

$$q_* \equiv \frac{\pi a^2 B_V}{R_0 I}, \quad \nu \equiv \frac{\beta_i q_*^2}{\epsilon}, \quad \mu \equiv 1 - M_{A\theta}^2, \quad \rho \equiv \frac{r}{a} \quad (15)$$

with  $I$  being the plasma current,  $\beta_i$  the toroidal  $\beta$ ,  $\mu$  a measure of the flow. Observe that  $\mu$  changes sign when the flow changes from sub- to super-Alfvénic. The constants  $A$  and  $C$  can now be related to physical quantities through straightforward algebra. The condition  $M_{A\theta} = 1$  ( $\mu = 0$ ) represents a singular point of Eq. (11), where Eq. (14) does not hold. Equation (14) can be used to determine the Shafranov shift of the plasma, which is determined by setting  $\nabla \Psi = 0$ , with the only caveat that the solution will be required to lie in the interval  $0 \leq \rho \leq 1$ . After trivial algebra, the Shafranov shift  $\rho_\Delta$  is given by

$$\rho_\Delta = \frac{-1 + \sqrt{1 + 3(\nu/\mu)^2}}{3(\nu/\mu)} \quad (\mu > 0, \theta = 0), \quad (16)$$

$$\rho_\Delta = \frac{1 - \sqrt{1 + 3(\nu/\mu)^2}}{3(\nu/\mu)} \quad (\mu < 0, \theta = \pi). \quad (17)$$

It is immediately evident that the shift will have opposite directions depending on the sign of  $\mu$ . In particular, for slow flows ( $\mu > 0$ ) the Shafranov shift will be directed outward, as per usual tokamak equilibria, while it will be directed inward for fast flows ( $\mu < 0$ ). Shafranov shifts computed from Eqs. (16) and (17) for an arbitrary value of  $\nu$  are presented in Fig. 3. It can be observed that the shift increases with increasing flow if  $M_{A\theta}$  is smaller than 1, while it decreases with increas-

ing  $M_{A\theta}$  for  $M_{A\theta}$  larger than 1, approaching 0 for very fast flows. A region of the  $M_{A\theta}$  axis has been excluded from the calculation, as it is in a regime above the equilibrium limits. The discussion of this issue is omitted for brevity. Let it just be noted that the equilibrium limit can be trivially computed from the vacuum solution of the simplified GS equation in a fashion similar to the computation for the Shafranov shift. The presence of a separatrix outside the plasma region will be briefly mentioned in the following section. As a conclusion to the present discussion, it should be mentioned that equilibria with inverted Shafranov shift such as the ones described in the present section will only exist where the GS equation is elliptic. For that reason, the present solution will not be valid when the poloidal flow is sufficiently high to make the total plasma velocity larger than the magnetofast speed.

## B. Numerical results

A numerical solution of the Grad Shafranov equation with super-Alfvénic flow can be obtained using a modified version of the code FLOW.

The first obviously necessary modification of the code is in the Bernoulli equation. The usual numerical solution implemented in FLOW assumes sub-Alfvénic flow, and therefore looks for a solution of the Bernoulli equation in the regime  $M_{A\theta} < 1$ . In order to obtain a solution in the super-Alfvénic regime, the root of the Bernoulli equation must be bracketed by the appropriate boundaries. By inspection, it is clear that a super-Alfvénic root will satisfy the inequality:

$$0 < \rho < \Phi^2. \quad (18)$$

Equation (18) is accurate enough for the Bernoulli solver to promptly converge to the desired solution.

The solution of the GS equation has been shown in the previous paragraph to have unusual features in the plasma (inverted Shafranov shift). The analysis of the vacuum solution, which has been omitted for brevity, also has unusual results. For that reason, a vacuum region surrounding the plasma will also be considered in the numerical results in the present paragraph. In the vacuum, the modified GS equation simply reduces to

$$\Delta^* \Psi = 0. \quad (19)$$

As for the plasma region, the modified GS equation described in Sec. II, and reproduced in here for convenience, needs to be solved:

$$\begin{aligned} \nabla \cdot \left[ (1 - M_{A\theta}^2) \left( \frac{\nabla \Psi}{R^2} \right) \right] = & - \frac{B_\varphi}{R} \frac{dF(\Psi)}{d\Psi} - \frac{\vec{v} \cdot \vec{B}}{\sqrt{\mu_0}} \frac{d\Phi(\Psi)}{d\Psi} \\ & - R\rho v_\varphi \frac{d\Omega(\Psi)}{d\Psi} - \rho \frac{dH(\Psi)}{d\Psi} \\ & + \frac{\rho^\gamma}{\gamma - 1} \frac{dS(\Psi)}{d\Psi}, \end{aligned} \quad (20)$$

where  $M_{A\theta}^2 = \Phi^2(\Psi)/\rho$ , and more details about the free functions have been given in Ref. 7. Since we are interested in the effects of poloidal flow, purely toroidal rotation is not

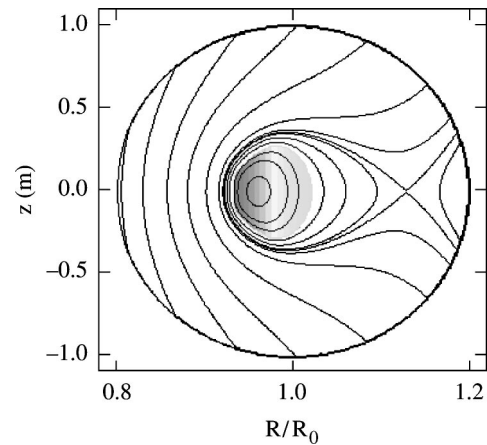


FIG. 4. FLOW super-Alfvénic equilibrium.

essential to the discussion. Toroidal velocity is therefore minimized by setting  $M_\varphi(\Psi) = 0$  or equivalently:

$$\Omega(\Psi) = - \sqrt{\gamma \frac{P(\Psi)}{D(\Psi)} \frac{M_\theta(\Psi)}{R_0}}. \quad (21)$$

Equation (21) also minimizes the total plasma velocity for a given poloidal velocity. It should also be noted that the existence of super-Alfvénic roots of the Bernoulli equation is not ensured for arbitrary flow, in a way similar to what happens for sub-Alfvénic roots, as described in Ref. 10. This means that the flow level will have to be adjusted, depending on the case, in order to both satisfy the ellipticity condition and allow for solution of the Bernoulli equation.

The next step is to assign the proper boundary conditions for Eqs. (19) and (20). As for the plasma region, the required bc is simply the continuity of  $\Psi$  across the plasma-vacuum interface. For the vacuum region, a condition is assigned on a prescribed surface. The external boundary can be interpreted as a superconducting wall, with the value of  $\Psi$  on the wall determined in order to reproduce the externally applied vertical field.

The last step is to prescribe the position of the plasma-vacuum interface. This is accomplished by assigning

$$\Psi_E = \alpha \Psi_{\text{MAX}}, \quad (22)$$

where  $\Psi_E$  is the value of  $\Psi$  at the plasma edge,  $\Psi_{\text{MAX}}$  the value of  $\Psi$  at the magnetic axis, assumed positive, and  $\alpha$  an arbitrary positive constant  $< 1$ . With the condition of Eq. (22), the position of the interface will depend on the solution, i.e., the code will be free boundary for the solution in the plasma region.

The first check that is performed with the simplified theory is represented in Fig. 4. The figure represents plasma density (gray scale) and the magnetic surfaces in both the plasma and the vacuum region. The inward Shafranov shift is clearly visible in the picture, and the presence of a separatrix in the vacuum region outboard of the plasma column is also apparent. This equilibrium is computed with the set of parameters listed in Table III. The free functions of  $\Psi$  are assigned in such a way that a roughly constant  $M_{A\theta}$  will result in the equilibrium. The free function  $F(\Psi)$ , related to the

TABLE III. FLOW equilibrium data.

Variable	Approximate value
$M_{A\theta}$	3
$\nu$	1.3
$q^*$	2

toroidal component of the magnetic field, is also assigned as a function of the flow and the pressure in a fashion similar to Eq. (12).

A more quantitative test of the results is performed next. As only the solution in the plasma has been discussed in the previous paragraph, the computational region is now restricted to the plasma, by setting  $\alpha=0$  in Eq. (22), therefore running the code in the customary fixed-boundary mode. The effects of the poloidal flow on the Shafranov shift in numerical equilibria are then examined. In order to do this, a careful evaluation of the simplified analytic theory presented in this work and of the general large aspect ratio theory of equilibria with macroscopic flow<sup>10</sup> is necessary, which allows to recognize the following points.

- (1) The analytic model assumes a constant  $M_{A\theta}$ , and therefore a quantitative comparison should be performed using  $M_{A\theta}$  as close as possible to a constant (as already done for the equilibrium in Fig. 4).
- (2) In the complete model,  $M_{A\theta}$  will depend on  $\Phi(\Psi)$  and the density  $\rho$ . The free function of  $\Psi$  can be assigned to be a constant, however the density will be given by the numerical solution of the Bernoulli equation.<sup>7</sup>
- (3) If  $M_{A\theta}$  is large, then  $M_{s\theta}$  will also be large, and the density will be given approximately by

$$\rho \approx D(\Psi) \left( \frac{R_0}{R} \right)^2. \quad (23)$$

- (4) A roughly constant density will therefore be obtained by assigning a constant  $D(\Psi)$  and using a large aspect ratio. Note, however, that the aspect ratio cannot be too large, as the effects described in this work are purely toroidal effects.

Following these considerations, a series of equilibria has been computed in a plasma with circular cross section and large aspect ratio.  $\beta_i$  has been chosen approximately equal to the inverse aspect ratio, and the (input) poloidal Alfvénic Mach number has been varied from 2 to 5. The Shafranov shifts computed by the code are then compared to the ones of the simplified model, given by Eq. (17). As neither  $\mu$  nor  $\nu$  are exact input parameters for the code, both have been computed from the numerical results of each equilibrium, and substituted back into the analytic formula for the Shafranov shift. The resulting shifts are plotted in Fig. 5. The curve labeled “Theory” has been obtained using the input Alfvénic poloidal Mach number and the one labeled “Theory (corrected  $M_{A\theta}$ )” with the average Alfvénic poloidal Mach number obtained from the code, also showing that the two are

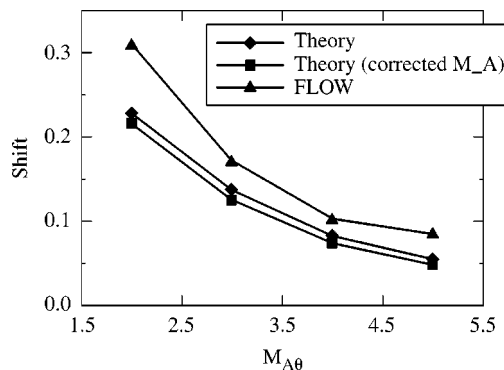


FIG. 5. Comparison between analytical and numerical Shafranov shift.

very close. Although the numerical shifts are larger than the analytical ones, there is good agreement between theoretical and numerical results.

The inward Shafranov shift can be easily explained by realizing that the net centrifugal force due to the plasma rotation can balance the outward-pointing pressure force. Indeed, if the flux surfaces are shifted inward the flow velocity increases in the inboard section of the plasma leading to a net centrifugal force directed along the major radius but in the inward direction. Such a force can balance the pressure force and keep the plasma in equilibrium.

## V. QUASI-OMNIGENOUS EQUILIBRIA WITH FAST POLOIDAL FLOW

As already observed in Sec. IV, the main obstacle for achieving fast poloidal flows is the high poloidal viscosity of tokamak plasmas. The poloidal viscosity is driven by the magnetic pumping<sup>15</sup> and decreases as the inverse of the square velocity for fast rotations.<sup>12</sup> The origin of the pumping is the variation of the magnetic field strength along the magnetic surfaces, or, in other words, the fact that the magnetic field strength is not a function of  $\Psi$  only. There exists however a class of equilibria, called “omnigenous,” in which the surfaces of constant  $|B|$  are exactly aligned with the surfaces of constant poloidal magnetic flux  $\Psi$ , i.e.,  $|B|=|B|(\Psi)$ . In a pioneering work by Palumbo,<sup>16</sup> it was shown that high  $\beta$  equilibria can reach such condition for static plasma. An expansion of the solution of Palumbo was later given by Bishop and Taylor,<sup>17</sup> which showed that isodynamic magnetic surface configurations also have the property to correspond to more than one plasma equilibrium. In later works, see e.g., Ref. 18, it was more strongly emphasized that omnigenous equilibria in closed systems require  $|B|$  to vanish on the magnetic axis in order to exist. Different is the situation in open field configurations, such as magnetic mirrors, which are however not relevant to the present discussion. The possibility of obtaining omnigenous equilibria in the presence of macroscopic flow has been investigated in the past by Tasso and Throumoulopoulos,<sup>19</sup> which ruled out the possibility of omnigenous equilibria for non-field-aligned flow in incompressible plasmas.

It has however been pointed out<sup>17</sup> that Palumbo-like omnigenous equilibria are likely not relevant to tokamaks, because of the vanishing magnetic field on the magnetic axis

and of the safety factor profile, which also vanishes on the magnetic axis. It seems therefore worthwhile to investigate the existence of quasi-omnigenous equilibria, in which  $|B|$  is a function of  $\Psi$  up to some small correction, to be quantified in the following. This class of equilibria will still have reduced magnetic pumping with respect to “nonomnigenous” equilibria, but without the defects of the “fully omnigenous” equilibria. The elements that will be retained in the following analysis are essentially the Bernoulli equation (4) and the GS equation (5), with the addition of the equation for  $B_\varphi$  (3). No additional equation is introduced at this point to impose omnigenity, which will follow from the equation ordering. The inverse aspect ratio  $\epsilon$  is chosen as the small expansion parameter. The magnetic field scaling is defined as  $B_\theta/B_\varphi \sim \epsilon$ , and  $B_\varphi$  is required to be  $B_\varphi(\Psi) + O(\epsilon^2)$ , from which immediately follows  $|B| = |B|(\Psi) + O(\epsilon^2)$ . For the ordering of the terms in the Bernoulli and GS equations, it is more convenient to rewrite the equations as in Ref. 10, namely,

$$\hat{B}^2 M_\theta^2(\Psi) X^{\gamma+1} - \left[ \frac{2}{\gamma-1} + M_\theta^2(\Psi) + [M_\theta(\Psi) - M_\varphi(\Psi)]^2 \right. \\ \left. \times (\hat{R}^2 - 1) \right] X^{\gamma-1} + \frac{2}{\gamma-1} = 0, \quad (24)$$

$$\left[ 1 - \frac{\mu_0 \rho v_\theta^2}{B_\theta^2} \right] \Delta^* \Psi + \frac{\partial}{\partial \Psi} \left( \frac{B_\varphi^2 R^2}{2} \right) + \mu_0 \frac{\partial p}{\partial \Psi} \\ + \frac{\mu_0 \rho v_\theta^2}{B_\theta^2} R^2 \frac{\partial}{\partial \Psi} \frac{B_\theta^2}{2} - \frac{\mu_0 \rho v_\varphi^2}{B_\theta^2} \frac{\nabla \Psi \cdot \nabla R}{R} = 0, \quad (25)$$

where  $M_\theta(\Psi)$  and  $M_\varphi(\Psi)$  are, respectively, the poloidal and toroidal quasisonic Mach numbers,  $X(\Psi, \chi)$  is defined by  $\rho(R, z) = D(\Psi)/X$ ,  $\hat{R} \equiv R/R_0$ , and  $\beta_\gamma \equiv \gamma \mu_0 P(\Psi)/B_0^2(\Psi)$ . Under the same token, Eq. (3) is also rewritten in terms of the free functions in Ref. 10, as

$$B_\varphi = \frac{B_0(\Psi)}{\hat{R}} \frac{1 - \hat{R}^2 \beta_\gamma(\Psi) M_\theta(\Psi) [M_\theta(\Psi) - M_\varphi(\Psi)]}{1 - X \beta_\gamma(\Psi) M_\theta(\Psi)^2}. \quad (26)$$

The ordering used to solve Eqs. (24)–(26) is then defined as follows. As the present work is focused on equilibria with high poloidal flow, the free function  $M_\theta(\Psi)$  is ordered to be  $M_\theta(\Psi) \sim 1/\sqrt{\epsilon}$ . For convenience, we also define  $\delta M(\Psi) \equiv M_\theta(\Psi) - M_\varphi(\Psi)$ , with  $\delta M(\Psi) \sim 1/\sqrt{\epsilon}$ . It is also convenient to define the ordering for the poloidal Alfvénic Mach number as  $1 - M_{A\theta}^2 \sim 1$ . Since  $M_{A\theta}$  can be written as  $M_{A\theta}^2 = X \beta_\gamma M_\theta^2$ , this implies  $X \beta_\gamma \sim \epsilon$ . As in Ref. 10,  $X$  is assumed to be of order 1, and therefore  $\beta_\gamma \sim \epsilon$ . In order to work with variables of order 1, and also to make the ordering explicit, we define “hatted” variables of order 1, namely,  $\hat{M}_\theta \equiv \sqrt{\epsilon} M_\theta$ ,  $\delta \hat{M} \equiv \sqrt{\epsilon} (\delta M)$ , and  $\hat{\beta}_V \equiv P(\Psi)/[\epsilon B_V^2]$ , where  $B_V$  is the vacuum field. Finally, for the sake of compactness in the following computations, we also define:

$$A(\Psi) \equiv \beta_\gamma(\Psi) M_\theta(\Psi) [M_\theta(\Psi) - M_\varphi(\Psi)] \sim 1, \\ C(\Psi) \equiv \beta_\gamma(\Psi) M_\theta^2(\Psi) \sim 1. \quad (27)$$

In order to achieve  $|B| = |B|(\Psi)$  up to corrections of order  $\epsilon^2$ , it is now necessary to solve Eq. (26) for  $B_\varphi$  up to order  $\epsilon$ .  $B_\varphi$  is then written as  $B_\varphi \simeq B_{\varphi 0}(\Psi) + \epsilon B_{\varphi 1}(\Psi)$ , with  $B_{\varphi 1} \sim B_{\varphi 0}$ . As  $X$  explicitly appears in Eq. (26), it will be also necessary to simultaneously solve Bernoulli equation (24) for  $X$ . In the same fashion as done for  $B_\varphi$ ,  $X$  is expanded in powers of  $\epsilon$  as  $X \simeq X_0 + \epsilon X_1$ , again with  $X_1 \sim X_0$ . It is important to emphasize that even though  $B_\varphi$  is required to be a function of  $\Psi$  only up to corrections of order  $\epsilon^2$ , a similar requirement does not hold for  $X$ . Indeed, it is precisely the fact that  $X$  is not only a function of  $\Psi$ , which will allow to cancel out the  $\theta$ -dependent  $\epsilon$  correction in  $B_\varphi$ . In this sense, compressibility is an essential element in our analysis.

Before proceeding with the solution of the equilibrium problem, it seems worthwhile to stress which are the unknowns that need to be determined, and which equations are available. The unknowns are essentially the free functions of  $\Psi$  in the equilibrium problem in the presence of flow, namely,  $M_\theta(\Psi)$ ,  $M_\varphi(\Psi)$ ,  $P(\Psi)$ ,  $D(\Psi)$ , and  $B_0(\Psi)$ , and the density  $\rho$ , which is expressed through the auxiliary variable  $X$ . The hatted variables  $\hat{M}_\theta$ ,  $\delta \hat{M}$ , and  $\hat{\beta}_V$  are used instead of  $P$ ,  $M_\theta$ ,  $M_\varphi$ , but is obviously trivial to obtain the last three from the previous ones. The equations used to determine the six unknowns are the definition of  $B_\varphi$  (26), Bernoulli equation (24), and the GS equation (25), all of which will be solved order by order in an  $\epsilon$  expansion.

The solution of the first two orders of Eq. (26) is trivial and can be written as

$$B_{\varphi 0} = B_0 \frac{1 - A}{1 - X_0 C}, \quad (28)$$

$$\epsilon B_{\varphi 1} = \epsilon \frac{B_0}{1 - X_0 C} \left[ -(1 + A) \cos \theta + \frac{(1 - A) X_1 C}{1 - X_0 C} \right] \\ \equiv \epsilon B_0 K(\Psi). \quad (29)$$

Equation (29) is a constraint equation for the omnigenity, which can be cast in a more convenient form using the solution of the Bernoulli equation. Bernoulli equation is also straightforward to solve up to order  $\epsilon$ , and the solution can be written explicitly as

$$X_0 = \frac{\pm 1}{1 - A \pm C}, \quad (30)$$

$$X_1 = \frac{X_0 \delta \hat{M}^2}{\hat{M}_\theta^2} \cos(\theta) + \frac{X_0 - X_0^{2-\gamma}}{(\gamma - 1) \hat{M}_\theta^2} - \left( \frac{1 - A}{1 - X_0 C} \right) K X_0^3. \quad (31)$$

It should not come as a surprise that the Bernoulli equation has more than one solution, as it is well known in the literature that it can have up to four solutions, two of which are sub-Alfvénic, and two super-Alfvénic. The choice of the “right” solution for  $X_0$  also depends on the explicit solutions for  $A$  and  $C$  [see below Eq. (35)], and its discussion is postponed until those solutions have been determined. Using Eq. (31), the quasiomnigenity condition can be cast in its final form, which reads

$$\frac{(1-A)C X_0 \delta \hat{M}^2}{1 - X_0 C \hat{M}_\theta^2} - (1+A) = 0. \quad (32)$$

From Eqs. (29) and (31) it is also possible to write the explicit definition of  $K(\Psi)$ :

$$K(\Psi) = \frac{(1 - X_0 C)(1 - A)C(X_0 - X_0^{2-\gamma})}{(\gamma - 1)\hat{M}_\theta^2[(1 - X_0 C)^3 + C(1 - A)^2 X_0^3]}. \quad (33)$$

The equations written so far are all that is needed in order to assure omnigenity in the first two orders in  $\epsilon$ . What is still

$$A = \frac{\delta \hat{M} \left[ 1 + 2\gamma \hat{M}_\theta \hat{\beta}_V (\hat{M}_\theta + \delta \hat{M}) \pm \sqrt{1 + 4\gamma \hat{M}_\theta \hat{\beta}_V (\hat{M}_\theta + \delta \hat{M})} \right]}{2\gamma \hat{M}_\theta \hat{\beta}_V (\hat{M}_\theta + \delta \hat{M})^2}, \quad (35a)$$

$$C = \frac{1 + 2\gamma \hat{M}_\theta \hat{\beta}_V (\hat{M}_\theta + \delta \hat{M}) \pm \sqrt{1 + 4\gamma \hat{M}_\theta \hat{\beta}_V (\hat{M}_\theta + \delta \hat{M})}}{2\gamma \hat{\beta}_V (\hat{M}_\theta + \delta \hat{M})^2}. \quad (35b)$$

The  $\pm$  signs in Eqs. (35) and (30) determine a total of four possible different values for  $X_0$ . In order to determine which  $X_0$  value to choose, the following requirements need to be met: (1)  $X_0$  has to be positive, and of order 1; (2)  $X_0 C$  (representing  $M_{A\theta}^2$  to lowest order in  $\epsilon$ ) also has to be positive, and  $\geq 1$ . Direct calculations show that usually at most one of the solutions meets both requirements. In the case that more than one does, the solution that gives  $X_0$  and  $X_0 C$  closest to 1 is chosen.

The analysis can now be completed by solving the first-order form of the GS equation  $\epsilon$  expansion. In order to do this, three different terms must be separately set to 0, namely, the sum of the terms proportional to  $\epsilon \cos(\theta)$ , the sum of the terms proportional to  $\partial R / \partial \Psi$ , and the sum of the  $\Psi$  derivative terms. The first of these [ $\epsilon \cos(\theta)$  terms] is automatically satisfied, while the other two (in that order) give the equations

$$\frac{\gamma \hat{\beta}_V \left( X_0 \hat{M}_\theta - \delta \hat{M} \right)^2}{X_0 (1 - C X_0)} = 1, \quad (36)$$

$$\left[ \left( \frac{1 - X_0 C}{1 - A} \right) K + \frac{\hat{\beta}_V}{X_0^\gamma} \right] = \alpha \quad (37)$$

with  $\alpha \sim 1$  being a free parameter, controlling the actual values that  $\hat{\beta}_V$  will be allowed to assume. Equations (32), (36), and (37) are three equations in the three unknowns  $\hat{M}_\theta$ ,  $\delta \hat{M}$ , and  $\hat{\beta}_V$ . A direct solution of Eqs. (32), (36), and (37) shows that an infinite set of solutions exists, and triplets of values ( $\hat{M}_\theta$ ,  $\delta \hat{M}$ ,  $\hat{\beta}_V$ ) can be easily computed with a standard solver for nonlinear algebraic equations for any given value of  $\alpha$ . Some numerical results are presented in Fig. 6 for  $\alpha = 0.75$ .

left to solve for is the equilibrium, which can be determined with a customary  $\epsilon$  expansion of the GS equation, with the only difference from the usual (static) theory that the flow terms also need to be taken into account. Order 0 of the GS equation is trivial, and it reduces to

$$\frac{\partial B_{\varphi 0}^2}{\partial \Psi} = 0 \rightarrow B_{\varphi 0} = B_V \rightarrow B_0(\Psi) = B_V \frac{1 - X_0 C}{1 - A}. \quad (34)$$

This eliminates  $B_0(\Psi)$  from the system, leaving the only unknowns  $\hat{M}_\theta$ ,  $\delta \hat{M}$ , and  $\hat{\beta}_V$ . From Eqs. (27), (30), and (34) it is also possible to explicitly determine  $A$  and  $C$  as

“Hatted” variables  $\hat{M}_\theta$ ,  $\delta \hat{M}$ ,  $\hat{\beta}_V$  are plotted, and  $X_0$  is included as well for illustration purposes.

Before the results so far obtained can be used as input for a numerical solution of the equilibrium problem, two more elements must be taken into account. First, as the GS equation has only been solved up to first order in  $\epsilon$ , the poloidal magnetic flux  $\Psi$  has not explicitly appeared anywhere in the solution. This is due to the fact that  $M_{A\theta}$  has been assumed to be of order 1. The immediately recognizable effect of this is that, given a set of values ( $\hat{M}_\theta$ ,  $\delta \hat{M}$ ,  $\hat{\beta}_V$ ) satisfying Eqs. (32), (36), and (37), such a set can be parametrized as a curve function of  $\Psi$  in the ( $\hat{M}_\theta$ ,  $\delta \hat{M}$ ,  $\hat{\beta}_V$ ) space. In other words, one of the functions  $\hat{M}_\theta$ ,  $\delta \hat{M}$ , and  $\hat{\beta}_V$  can be actually assigned as a free function of  $\Psi$ , while the other two will be automatically determined. In the following it is found convenient to assign  $\hat{\beta}_V(\Psi)$ , and therefore  $P(\Psi)$ . Second, looking back at Eq. (12), it can be noticed that one free function that has been introduced at that point, namely

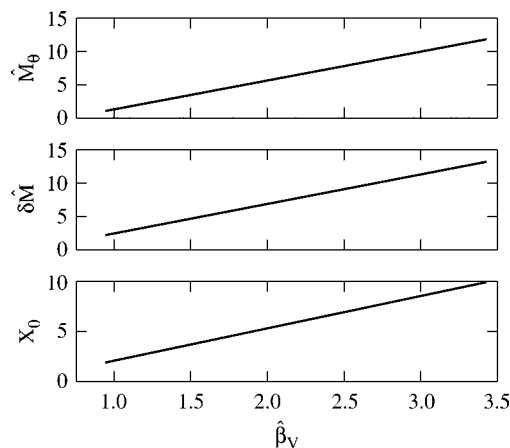


FIG. 6. Free functions  $\hat{M}_\theta$  and  $\delta \hat{M}$  and Bernoulli equation solution  $X_0$  as functions of  $\hat{\beta}_V$ .

$B_{\varphi 2}(\Psi)$ , has so far neither appeared nor has been assigned. Indeed, the 0th order term of  $B_{\varphi}$  has to be constant [see Eq. (34)], while the first-order term balances the pressure [Eq. (37)], exactly as in Eq. (12). This drives to the conclusion that  $B_{\varphi 2}(\Psi)$  is still a free function of  $\Psi$ , which will prove crucial in determining the actual equilibrium.

One last consideration seems at this point useful, which can be introduced considering Fig. 6. The figure shows numerical results for a reasonable, consistent with the ordering, range of values of  $\hat{\beta}_V$ ,  $\hat{M}_{\theta}$ ,  $\delta\hat{M}$ , and  $X_0$  also have reasonable values, even though for larger values of  $\hat{\beta}_V$  they appear to stretch beyond the proper limit of validity of our solution, if the expansion parameter  $\epsilon$ , which has so far been left unspecified, is assumed to have a realistic value. This naturally raises the question, whether the solution can be extended beyond its strict range of validity, and with what consequences. In particular, one would desire to obtain a solution with vanishing plasma pressure at the edge, in order to be able to assign realistic profiles to the free functions of  $\Psi$ . It should however be intuitive that the present solution, regardless of the ordering for  $\beta$ , cannot hold for vanishing plasma pressure. The reason is in the magnetic field ordering. As the poloidal field is ordered to be  $B_{\theta} \sim \epsilon B_{\varphi}$ , it will not appear in  $|B|$  up to order  $\epsilon^2$ . The vacuum toroidal field, to which the plasma field reconnects at the edge, is however proportional to  $1/R$ , i.e., it will have variations of order  $\epsilon$  from the inboard to the outboard side. As those variations cannot be compensated in  $|B|$  neither by the plasma, which has vanishing pressure, nor by the poloidal field, which is scaled to be small, it follows that a quasi-omnigenous solution like the one under examination cannot be extended to vanishing plasma pressure. This is indeed verified by the numerical solution of the system of Eqs. (32), (36), and (37), as the numerical solver fails for values of  $\hat{\beta}_V$  smaller than roughly  $1.2\alpha - 1.3\alpha$ , regardless of  $\alpha$ . Still concerning the plasma pressure, and the possibility of obtaining equilibria with small, even if not vanishing, pressure at the plasma edge, another element, which could be counterintuitive, must still be considered, i.e., the fact that the actual plasma pressure is given by  $p = P(\Psi)/X^{\gamma}$ . Observing again Fig. 6, it can be noticed that  $X_0$  varies faster than  $\hat{\beta}_V$ . This allows to conclude that a solution with pressure increasing from the plasma edge to the center will have *decreasing*  $P(\Psi)$  from the edge to the center, if all free functions are assigned according to the quasi-omnigenous solution presented in here.

This can be easily verified by solving an equilibrium with the code FLOW. As mentioned before, it is more interesting to calculate equilibria, in which the plasma pressure and density have profiles decreasing, rather than increasing, from the plasma center to the edge. Even though, for the reasons explained in the present section, it is not possible to extend our solution to vanishing pressures, it is however possible to obtain lower pressures, by assigning an input with increasing  $X$  as one moves away from the plasma center. This can simply be done by selecting a larger interval  $\hat{\beta}_{V_{\min}} < \hat{\beta}_V < \hat{\beta}_{V_{\max}}$  for generating the code input. In doing so, one should remember that our solution is not valid for large  $X$ , or

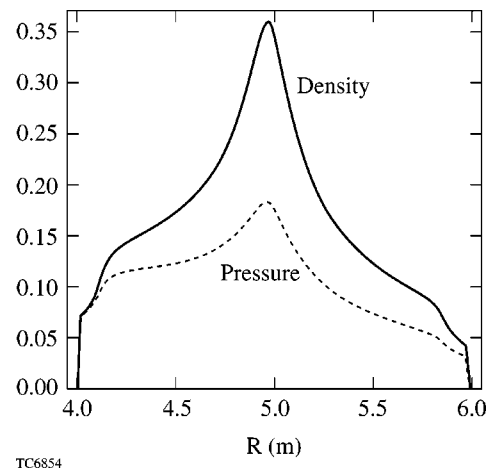


FIG. 7. Density and pressure line-cuts in a quasi-omnigenous equilibrium with peaked profiles.

large  $M_{A\theta}$ . This could mean that the quasi-omnigenous properties of the plasma could only hold in the center of the computational region, where the analytical solution assumptions are satisfied. In a sense, this is not dissimilar from what we would expect in an experiment, if a plasma with the properties here described could be obtained. Indeed, in an experiment pressure and density will eventually have to vanish, and the equilibrium will have to assume some different characteristics, which we are not describing here, since they are localized near the edge. It is easy to imagine that our free functions can be prolonged in some way to obtain vanishing pressure at the edge, obviously violating the quasi-omnigenicity condition near the edge. As we are focusing our attention on quasi-omnigenous regions, we will therefore limit the plasma region to have an input obtained from Eqs. (32), (36), and (37), and decreasing pressure moving away from the magnetic axis.

In order to obtain such equilibrium, we solve Eqs. (32), (36), and (37) for  $\alpha = 2.75$  and  $5 < \hat{\beta}_V < 25$ , and use the resulting free functions as input for the code. In order to extend the region of quasiomnigenicity, we assign  $\hat{\beta}_V(\Psi)$ , and therefore  $P(\Psi)$ , to decrease rapidly at the plasma edge and vary slowly in the plasma center. For convenience, the free function  $D(\Psi)$  is assigned to be a constant,  $D(\Psi) = 1$ , and the magnetic permeability is set to be  $\mu_0 = 1$ . All other free functions are derived from the solution of Eqs. (32), (36), and (37). The only exception to this is the free function  $B_0$  (quasitoroidal magnetic field), which is determined to order  $\epsilon$  by the analytical solution, but for which a degree of freedom is still present, namely, in the choice of  $B_{\varphi 2}$ .  $B_{\varphi 2}$  is simply assigned as a linear function of  $\Psi$ , decreasing from the edge to the center, namely,  $B_{\varphi 2} = -2\Psi/\Psi_c$ . The plasma cross section is assigned to be circular, with a minor radius  $a = 1$  and  $\epsilon = 1/5$ .

The numerical results obtained for such equilibrium are presented in Figs. 7 and 8. In Fig. 7, a line cut for density and pressure is presented. As it might have been expected from the previous discussion, both profiles are peaked in the plasma center and decreasing toward the edge, even though for both quantities the minimum values are of the same order

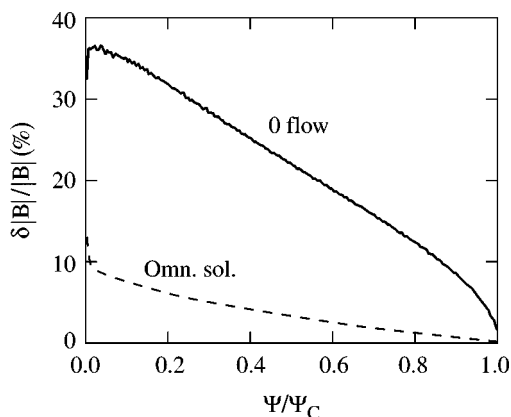


FIG. 8. Variation  $\delta|B|/|B|$  for a quasi-omnigenous equilibrium (dashed line) and a corresponding static equilibrium (solid line).

as the maximum values. What is more interesting to verify is, however, the magnetic field variation  $\delta|B|/|B|$ .

Figure 8 shows a comparison between a quasi-omnigenous and a static equilibrium, both with roughly the same pressure profile. The dashed line represents  $\delta|B|/|B|$  for the quasi-omnigenous equilibrium, while the continuous line represents the same variation for the static equilibrium. On the  $x$  axis of the picture is the magnetic flux  $\Psi$ , normalized to its maximum value, with 0 corresponding to the plasma edge and 1 to the magnetic axis. It is clearly visible in the picture that the quasi-omnigenous solution has a much lower variation than the corresponding static equilibrium. It can also be observed that the maximum variation in the static equilibrium is close to 40%, i.e.,  $2\epsilon$ , as expected. For the quasi-omnigenous equilibrium, a deviation of the order of  $\sim\epsilon^2\sim 4\%$  is expected, and the figure shows that the deviation is  $\leq 5\%$  in the larger part of the plasma. The analysis of the code output also shows that  $|B_\theta| \ll |B|$ , thus indicating that the magnetic fields satisfy the required ordering.

## VI. CONCLUSIONS

Tokamak equilibria in the presence of macroscopic flow greatly differ from static equilibria. In particular, the presence of sufficiently fast poloidal flow can give rise to qualitative changes in equilibrium properties. The discontinuities arising in the presence of transonic poloidal flows, due to the transition between the subsonic and the supersonic regime,

lead to a pedestal structure in the pressure and density profiles. In the present work, it has been emphasized that only slow velocities are necessary in order to obtain transonic equilibria. Much faster flows, in particular flows in the range of the poloidal Alfvén speed, are probably out of the reach of present days experiments. The existence of equilibria with such high rotations has however been proved in the present work with numerical and theoretical tools. As high rotations will require a large drive, it is not realistic to think they could be reached in experiments, unless some technique to reduce the neoclassical poloidal viscosity is also introduced. Here we have shown that an appropriate choice of the free functions of  $\Psi$  assigning the equilibrium properties can be used to that effect.

## ACKNOWLEDGMENTS

The authors kindly thank Dr. J. Manickam, Dr. S. Kaye, Professor J. P. Freidberg, and Dr. J.-L. Gauvreau for their useful contributions.

This work was supported by the U.S. Department of Energy under Contract No. DE-FG02-93ER54215.

- <sup>1</sup>R. J. Taylor, J.-L. Gauvreau, M. Gilmore, P.-A. Gourdain, D. J. LaFonteese, and L. W. Schmitz, *Nucl. Fusion* **42**, 46 (2002).
- <sup>2</sup>S. K. Erents, A. V. Chankin, G. F. Matthews, and P. C. Stangeby, *Plasma Phys. Controlled Fusion* **42**, 905 (2000).
- <sup>3</sup>T. S. Taylor, H. St. John, A. D. Turnbull *et al.*, *Plasma Phys. Controlled Fusion* **36**, B229 (1994).
- <sup>4</sup>M. Ono, S. M. Kaye, Y.-K. M. Peng *et al.*, *Nucl. Fusion* **40**, 557 (2000).
- <sup>5</sup>S. Semenzato, R. Gruber, and H. P. Zehrfeld, *Comput. Phys. Rep.* **1**, 389 (1984).
- <sup>6</sup>A. J. C. Beliën, M. A. Botchev, J. P. Goedbloed, B. van der Holst, and R. Keppens, *J. Comput. Phys.* **182**, 91 (2002).
- <sup>7</sup>L. Guazzotto, R. Betti, J. Manickam, and S. Kaye, *Phys. Plasmas* **11**, 604 (2004).
- <sup>8</sup>E. Hameiri, *Phys. Fluids* **26**, 230 (1983).
- <sup>9</sup>R. Iacono, A. Bondeson, F. Troyon, and R. Gruber, *Phys. Fluids B* **2**, 1794 (1990).
- <sup>10</sup>R. Betti and J. P. Freidberg, *Phys. Plasmas* **7**, 2439 (2000).
- <sup>11</sup>K. C. Shaing, E. C. Crume, Jr., and W. A. Houlberg, *Phys. Fluids B* **2**, 1492 (1990).
- <sup>12</sup>A. B. Hassam, *Nucl. Fusion* **36**, 707 (1996).
- <sup>13</sup>J. P. Freidberg, *Ideal MHD* (Clarendon, Oxford, 1987) p. 138ss.
- <sup>14</sup>F. A. Haas, *Phys. Fluids* **15**, 141 (1972).
- <sup>15</sup>A. B. Hassam and R. M. Kulsrud, *Phys. Fluids* **21**, 2271 (1978).
- <sup>16</sup>D. Palumbo, *Nuovo Cimento B* **53**, 507 (1967).
- <sup>17</sup>C. M. Bishop and J. B. Taylor, *Phys. Fluids* **29**, 1144 (1986).
- <sup>18</sup>M. P. Bernardin, R. W. Moses, and J. A. Tataronis, *Phys. Fluids* **29**, 2605 (1986).
- <sup>19</sup>H. Tasso and G. N. Throumoulopoulos, *Phys. Plasmas* **5**, 2378 (1998).